*Exploration Geophysics (2005) **36**, 18–25*
Butsuri-Tansa (Vol. 58, No.1)
Mulli-Tamsa (Vol. 8, No.1)

A simple approach to refraction statics with the Generalized Reciprocal Method and the Refraction Convolution Section

Derecke Palmer[1] **Leonie Jones**[2]

Key Words: Statics, reflection, refraction, GRM, RCS, seismic

ABSTRACT

We derive refraction statics for seismic data recorded in a hard rock terrain, in which there are large and rapid variations in the depth of weathering. The statics corrections range from less than 10 ms to more than 70 ms, often over distances as short as 12 receiver intervals. This study is another demonstration of the importance in obtaining accurate initial refraction models of the weathering in hard rock terrains in which automatic residual statics may fail.

We show that the statics values computed with a simple model of the weathering using the Generalized Reciprocal Method (GRM) and the Refraction Convolution Section (RCS) are comparable in accuracy to those computed with a more complex model of the weathering, using least-mean-squares inversion with the conjugate gradient algorithm (Taner et al., 1998). The differences in statics values between the GRM model and that of Taner et al. (1998) systematically vary from an average of 2 ms to 4 ms over a distance of 8.8 km. The differences between these two refraction models and the final statics model, which includes the automatic residual values, are generally less than 5 ms. The residuals for the GRM model are frequently less than those for the model of Taner et al. (1998). The RCS statics are picked approximately 10 ms later, but their relative accuracy is comparable to that of the GRM statics.

The residual statics values show a general correlation with the refraction statics values, and they can be reduced in magnitude by using a lower average seismic velocity in the weathering. These results suggest that inaccurate average seismic velocities in the weathered layer may often be a source of short-wavelength statics, rather than any shortcomings with the inversion algorithms in determining averaged delay times from the traveltimes.

INTRODUCTION

Statics, the corrections for variations in the elevation of the ground surface and for seismic wave propagation through the weathered layer, are an integral component in the processing of virtually all seismic reflection data recorded on land. They are particularly important for regional surveys in hard rock terrains. The seismic lines are usually set out perpendicular to the geologic strike and since a wide range of geologic units can be encountered, the thickness of the weathered layer and the seismic velocities in both the weathered and sub-weathering layers can be quite variable (Palmer et al., 2000, Figure 2). In such surveys, statics corrections are heavily reliant on a good first approximation with refraction methods, because reflection data in hard rock terrains do not always display the good lateral continuity required for fine-tuning with residual statics routines.

In this paper, we describe a simple approach to determining refraction statics with the generalized reciprocal method (GRM) (Palmer, 1980; Palmer, 1986) using a spreadsheet, and with the refraction convolution section (RCS) (Palmer, 2001a; Palmer, 2001b). The GRM and RCS statics solutions are then compared with the statics corrections computed with a least-mean-square inversion approach with the conjugate gradient algorithm (Taner et al., 1998). In general, there is excellent agreement. The significance of these results is that simple models for generating refraction statics are often adequate, even in areas of quite variable weathering.

The set of data we have used in this study is taken from the western part of Line 99AGS-L2 from the 1999 Lachlan Seismic Survey (L151) acquired for the Australian Geodynamics Cooperative Research Centre (AGCRC) and the New South Wales Department of Mineral Resources (NSWDMR) by the Australian National Seismic Imaging Resource (ANSIR). Survey L151 crossed part of the Palaeozoic Lachlan Fold Belt near West Wyalong, NSW (Glen et al., 2000). In the survey area, the bedrock topography is controlled by both variable in-situ weathering and the palaeo-drainage system of the Lachlan River. Figure 1 is a cross section computed as part of this study, and it shows large and rapid variations in depths up to 150 m to slightly weathered bedrock. In many places, shallow depths of weathering correlate with areas of elevated surface topography.

Approximately 100 shot records, representing 8.8 km of the seismic profile, were used in this study. The data were acquired with 240-channel split spreads using 40-m end-to-end groups, and three IVI Hemi-60 vibrators, 15 m pad to pad with a 10-m move-up. Three 10-s 6–90 Hz mono-sweeps with an 80-m VP interval were used.

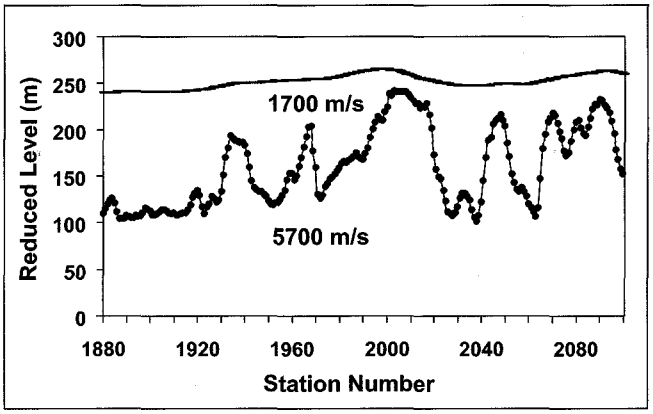

Fig. 1. Model of the weathered layer computed with the GRM for part of line 2, and using average seismic velocities of 1700 m/s in the weathering and 5700 m/s in the sub-weathering. Shallow depths of weathering frequently occur under areas of locally elevated topography.

[1] *School of Biological, Earth and Environmental Sciences, University of New South Wales, Sydney NSW 2052, Australia*
Email: D.Palmer@unsw.edu.au

[2] *Geoscience Australia*
GPO Box 378, Canberra ACT 2061, Australia
Leonie.Jones@ga.gov.au

Manuscript received November 2, 2004.
Revised manuscript received November 30, 2004.

DETERMINATION OF THE STATICS MODEL

The first-arrival refraction times were picked with a routine within the seismic reflection processing software. The first strong peak representing the Klauder wavelet was chosen.

The refraction statics method of Taner et al. (1998) assumes that the solution for the delay times at each station can be divided into a long-wavelength component resulting from the topography of the refractor, and a short-wavelength component due to variations in the seismic velocity and thickness of the near-surface layers. The separation into the two components is accomplished by smoothing within a window of radius similar to that of a Fresnel zone. The Fresnel zone is taken as the minimum size of the zone on the refractor that can be detected in the first arrivals received at the surface (Taner et al., 1998).

Jones and Drummond (2001) computed Fresnel zones using the model of Kvasnicka and Cerveny (1996), with an average seismic velocity of 1700 m/s in the upper layer and 5700 m/s within the refractor. The contrast in the seismic velocities is large and results in a critical angle of 17°. The computed Fresnel zone radius varied from 75 m to 150 m for refractor depths from 50 m to 150 m. A value of 100 m was adopted as a representative value.

Jones and Drummond (2001) then compared final stacked sections using refraction statics computed with smoothing radii of 400 m, 100 m, and 40 m, with and without automatic residual statics. They demonstrate that there is a marked improvement in the stacked section when the smoothing radius is reduced from 400 m to 100 m, but that there is little improvement with a 40 m radius. In each case, the application of residual statics improved the stack, although it was not as effective with the section computed using statics with the 400 m smoothing radius.

We derived the final statics model by combining the automatic residual statics with the original refraction model for comparison with the GRM and RCS statics models.

THE GRM STATICS MODEL

The model of the weathering used in the GRM approach to refraction statics consists of a single weathered layer above an unweathered layer, separated by an irregular interface. Often the weathered layer may in fact consist of a number of layers, each with a different seismic velocity. However, a single layer with an average velocity is employed, as it is usually not possible to specify a unique layered model. This is because of fundamental deficiencies with most sets of refraction data (Palmer, 2001c, p.659–660), rather than any limitations with the GRM, which can readily accommodate multi-layered weathering profiles (Palmer, 1980). In addition, the finite lengths of source and receiver arrays reduce the accuracy of first arrivals from the near-surface layers. We make no particular distinction between short- and long-wavelength refraction statics, although we recognize that a short-wavelength component can be recovered with automatic residual routines.

The refraction model used with the GRM separates the traveltime between each source and each receiver into the averages of the forward and reverse delay times at the source and the receiver, and the traveltime in the refractor (Palmer, 1986, p.106–107). It is described in equation 1 and illustrated in Figure 2.

$$T_{AY} = D_{Si} + D_{Rj} + AY/V_n \qquad (1)$$

The seismic velocity in the refractor V_n may vary laterally, in which case the last term in equation 1 is replaced with the appropriate summation.

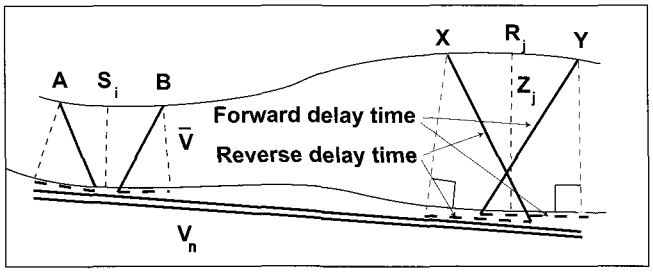

Fig. 2. The GRM refraction model of the weathering. The time-depth at R_j is the average of the delay times at X and Y. The ray paths shown represent *twice* the traveltime from source A to receiver Y.

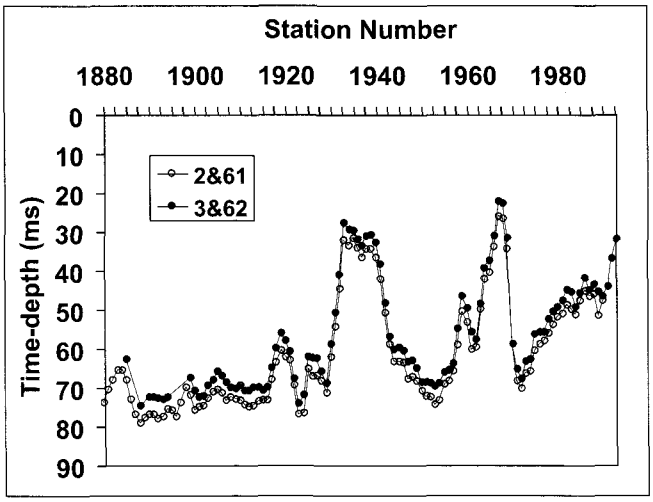

Fig. 3. Time-depths computed with two pairs of adjacent source points. These two profiles show the same relative time-depths, but they are separated by approximately 3.5 ms.

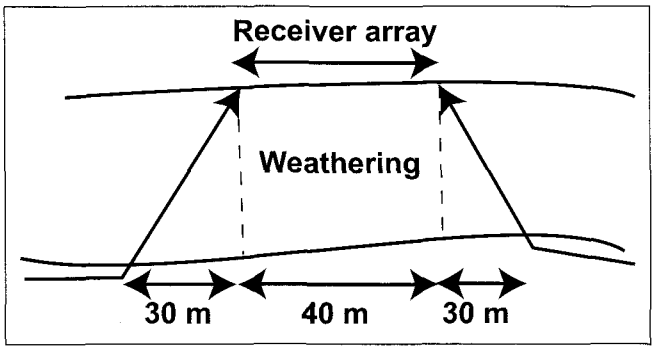

Fig. 4. Forward and reverse ray paths that demonstrate that the ends of the receiver arrays are the effective detection points for single receiver arrays of finite length. A substantial segment of the refractor is averaged when the lengths of the receiver array and the offset distances are considered.

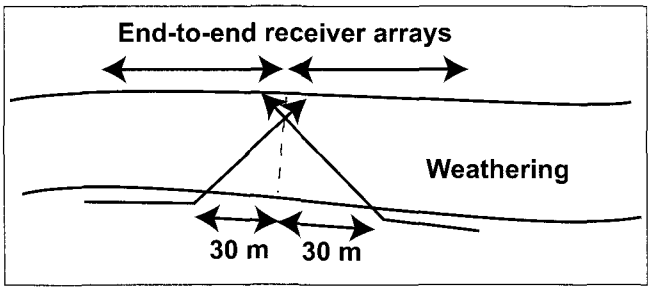

Fig. 5. Forward and reverse ray paths that demonstrate that the ends of the receiver arrays are the effective reference points when the traveltimes from adjacent end-to-end receiver arrays are used. The segment of the refractor that is averaged is reduced to twice the offset distance.

This refraction model is in fact that used by all inversion methods that employ forward and reverse traveltime data, including that of Taner et al. (1998). If the refractor interface is irregular and hence has segments that dip, then the forward and reverse delay times can differ. Therefore, when a single parameter is derived it is, by default, an average. The obvious benefit of determining averaged delay times is that a single value is obtained for each receiver. In addition, the depth conversion factor, which converts average delay times to depths (equation 3), is essentially independent of dip angles and therefore the horizontal layer approximations (equations 4 and 5), which are simple and convenient, can be used.

The advantage of using the GRM is that the algorithms provide an exact analysis of the traveltimes into averaged delay times. This is achieved by explicitly identifying the forward and reverse traveltimes within each algorithm. Accordingly, the traveltime data are processed in pairs of shot records. The time-depth algorithm (Palmer, 1986, equation 8.6 and Figure 8-4), which determines the averaged delay time at each detector, is given in equation 2.

$$D_{Rj} = \left(T_{S1\,RY} + T_{S2\,RX} - \left(T_{S1S2} + XY/V_n\right)\right)/2 \qquad (2)$$

This algorithm incorporates the separation of source and receiver delay times, refraction migration and convergence corrections of the standard delay time method (Gardner, 1939; Gardner, 1967; Barry, 1967), into a single convenient operation (Palmer, 1986, p.90–94). In this paper, we use the terms time-depth and averaged delay time synonymously.

We generated time-depth profiles from reversed pairs of shot records, starting with the two shot records which were located between the source points at stations 1872 and 1992. Although there are 120 stations between these two source points, only 118 traces were available because of a three-trace gap at each source point. This was further reduced to 116 stations with the application of a refraction migration distance of two station intervals or 80 m, in order to determine the static over a limited region under the centre of each receiver array, as is described below.

In practice, the reciprocal time $T_{S1\,S2}$, which is the traveltime from source S_1 to source S_2, is normally a constant for a given pair of sources. However, the reciprocal time is usually determined at the receiver most distant from the source, and as a result, it can be one of the most inaccurate (Palmer, 1986, p.156–162). Therefore, while the relative values between receivers are accurate, the absolute values determined with equation 2 may be in error.

The effects of reciprocal time errors are shown in Figure 3, in which the time-depths are plotted for two adjacent pairs of sources. It is clear that the two relative time-depth profiles of the refractor are similar, and that there is a separation of about 3.5 ms between the two profiles.

The correction to one of the reciprocal times is simply twice the average difference between the two time-depth profiles. Since there were often more than 110 pairs of overlapping time-depths, the accuracy in computing the reciprocal time correction is usually quite high. This operation also accommodates the XY/V_n term in equation 2. The time-depths corrected for reciprocal time errors are then averaged. At each end of the 220 stations of Line 2 which are used in this study, as few as four or five time-depth values were averaged, while in the centre, as many as 50 time-depth values were used. Those values that were clearly outliers were deleted, and as a result, the standard deviations of the averaged time-depths are generally less than one sample interval, which is two milliseconds.

ACCOMMODATING THE RECEIVER ARRAY

It is standard practice to reference each seismic trace to the centre of each receiver array. While this is a reasonable strategy for reflected signals that propagate predominantly in the vertical direction, it is not necessarily the case with the predominantly horizontally propagating refracted signals.

Figure 4 demonstrates the interval of the refractor interface that is effectively sampled with receiver arrays of finite length. For refracted signals travelling in the forward direction, that is, the source is on the left-hand side, the detector at the left-hand end of the array is the first to receive the energy, and therefore, the first-arrival time is appropriate to that detector. Similarly, for the reverse arrival from a source on the right-hand side, the receiver on the right-hand end of the array is the first to receive the energy, and therefore, the first-arrival time is appropriate to that detector.

Using an average depth of weathering of 100 m, the offset distance, which is the horizontal separation between the point of refraction on the interface and the point of emergence at the surface, is 100 tan(17°) or 30.6 m. Therefore, time-depths computed without any accommodation of the finite length of the receiver array, which in this study is 40 m, represent values that can effectively sample more than 100 m of the refractor interface.

The effect of the finite length of the receiver array can be removed with the application of refraction migration with an XY value of 40 m or one station interval. With this operation, the forward traveltime for a given receiver array is used with the reverse traveltime for the receiver array to the left. The arrivals then refer to the end of the receiver array as shown in Figure 5, and the length of the refractor interface that is averaged is reduced to about 60 m.

The time-depths at the end of each receiver array facilitate the computation of static values at the end of each receiver array, using the method described below, and in turn, the computation of differential statics across each receiver array. Figure 6 shows that differential statics caused by the finite length of the receiver array are commonly between 5 and 10 ms. Such differentials can be as significant a limitation of resolution as the accuracy of the statics themselves.

Clearly, it is necessary to determine a static that is more representative of the whole receiver array, such as a value that is applicable to the centre of the array. This can be achieved simply with a running average of adjacent values computed with the *XY* value of 40 m or one station interval.

Alternatively, it can be achieved with a refraction migration of 2 station intervals or 80 m, as shown in Figure 7. The benefit of this operation is that the length of the refractor interface that is averaged is reduced to an interval of about 20 m under the centre of each receiver array.

Figure 8 shows the time-depths computed with *XY* values of 0, 40 m, and 80 m. It is interesting to note that the values computed with *XY* values of 0 and 80 m are approximately midway between those computed with a 40 m XY value. Furthermore, the values computed with 0 and 80 m *XY* values are very similar, which is consistent with each averaging regions of the refractor under the centre of each receiver array.

THE REFRACTION CONVOLUTION SECTION

We generated individual RCSs from the same pairs of reversed shot records as we used in the computation of time-depths with the

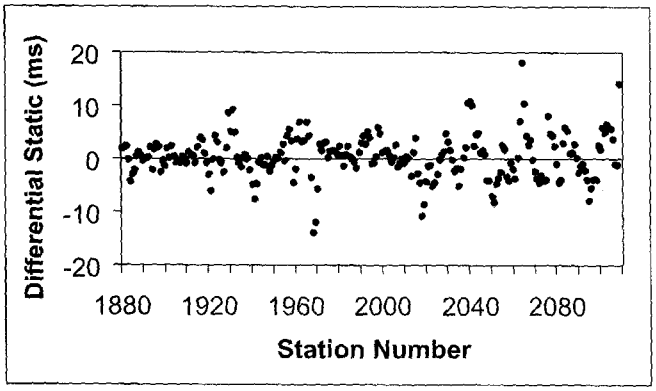

Fig. 6. Differences in statics corrections between the ends of each receiver array, obtained from the time-depths computed with a 40 m *XY* value. The differential statics commonly exceed 5 ms and they are an important factor limiting the achievable resolution.

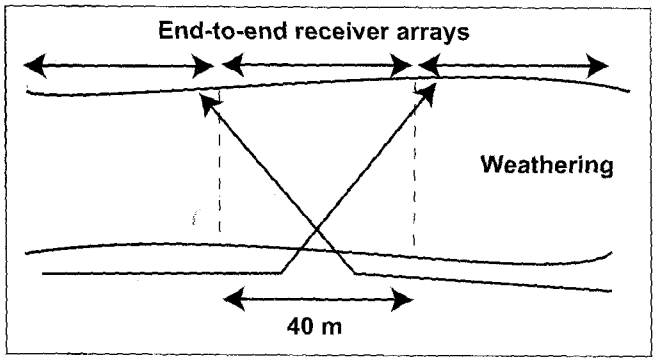

Fig. 7. Forward and reverse ray paths used to compute time-depths with an 80 m *XY* value. By using the arrivals at the adjacent receiver arrays, the segment of the refractor that is averaged is reduced to a minimum, and it occurs approximately in the centre of the middle receiver array.

GRM. Figure 9 shows the forward half of a shot record, which when convolved with the reverse half of the shot record in Figure 10, produces the RCS in Figure 11. The traces at each end of the RCS exhibit large amplitudes due to strong first-arrival energy and possibly correlation noise and as a result, each RCS has undergone trace balancing.

Figure 12 is more typical of the 50 RCSs generated as part of this study. Some traces exhibit quite high noise levels, mainly caused by vehicular traffic along the survey line. None of these traces has been edited: all traces have been included within the final stacked RCS shown in Figure 13.

Figure 13 also shows the fold of the stacked RCS. It varies from six fold at each end of the line to fifty fold in the centre. Time-depths have been measured at the first trough, and therefore occur about 10 ms after the times computed with the GRM using the picked traveltimes.

REPLACEMENT OF THE WEATHERED LAYER

Statics computations consist of two components. They are the correction for the weathered layer, and the correction for variations in topography from a datum. The approach adopted in this study replaces, rather than removes, the weathered layer with a layer of equivalent thickness but with the seismic velocity of the sub-weathering.

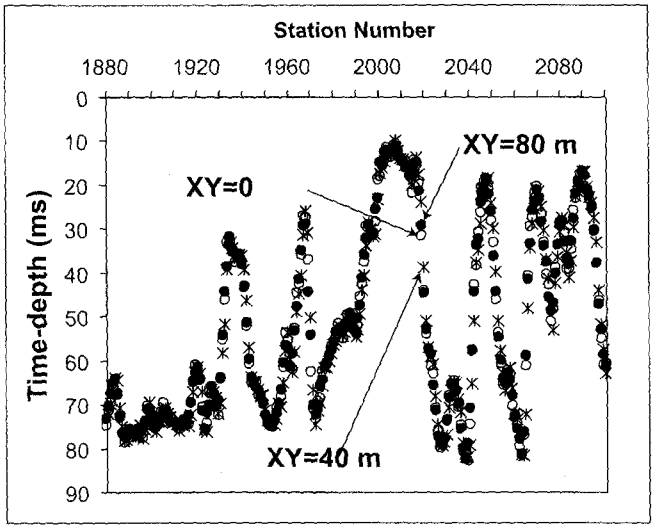

Fig. 8. Time-depths computed with *XY* values of 0 (open circles), 40 m (crosses) and 80 m (opaque circles). There is close similarity between the values computed with 0 and 80 m *XY* values. The values computed with a 40 m *XY* value represent averaged delay times at the ends of the receiver arrays, and they are often midway between the values computed with 0 and 80 m *XY* values.

The thickness of the weathered layer Z_{Rj} is given by

$$Z_{Rj} = D_{Rj} DCF \ , \tag{3}$$

where *DCF*, the depth conversion factor relating the time-depth and the depth, is given by

$$DCF = V_n V / \left(V_n^2 - V^2\right)^{1/2} \ , \tag{4}$$

or

$$DCF = V / \cos i \ , \tag{5}$$

where V is the average seismic velocity in the weathered layer and

$$\sin i = V / V_n \ . \tag{6}$$

The vertical traveltime through the weathered layer is

$$t_{\text{vertical}} = Z_{Rj} / V \ . \tag{7}$$

This time is replaced with one in which the seismic velocity is that in the sub-weathering, that is, with the traveltime

$$t_{\text{replacement}} = Z_{Rj} / V_n \ . \tag{8}$$

Therefore, the weathering correction subtracts the vertical traveltime and substitutes it with the replacement time, i.e.,

$$\text{Weathering correction} = t_{\text{vertical}} - t_{\text{replacement}} = D_{Rj} K \ , \tag{9}$$

where

$$K = \left[\left(1 - V / V_n\right) / \left(1 + V / V_n\right)\right]^{1/2} \ . \tag{10}$$

This approach scales the time-depth with the number K, which is less than 1. For an average seismic velocity in the weathering of 1700 m/s and an average seismic velocity in the sub-weathering of 5700 m/s, K is 0.735 .

The second component of the static is the elevation term. It is the difference between the elevation of the receiver array and the datum, divided by the seismic velocity in the sub-weathering.

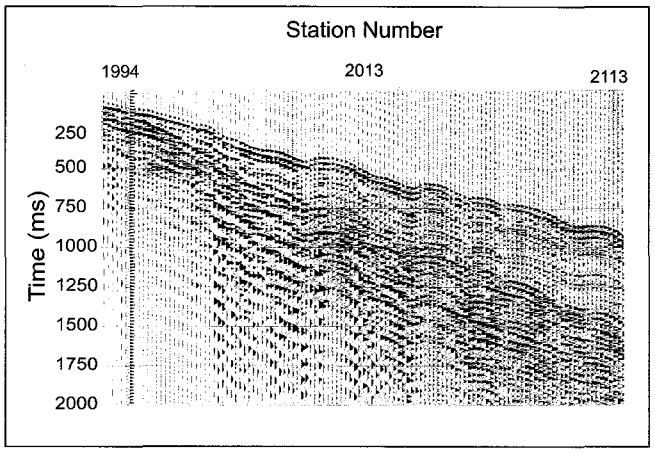

Fig. 9. Forward shot record used to compute the RCS in Figure 11.

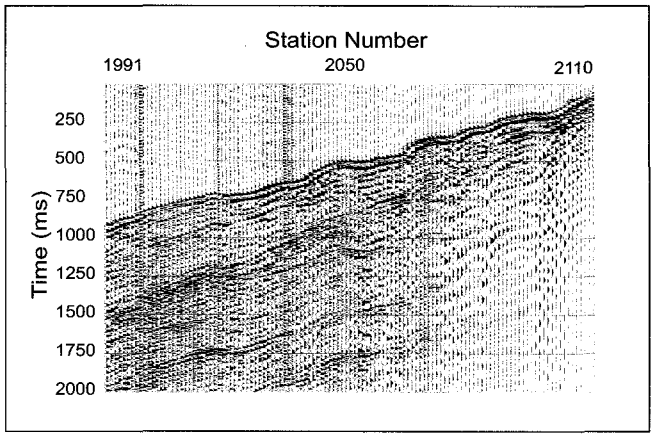

Fig. 10. Reverse shot record used to compute the RCS in Figure 11.

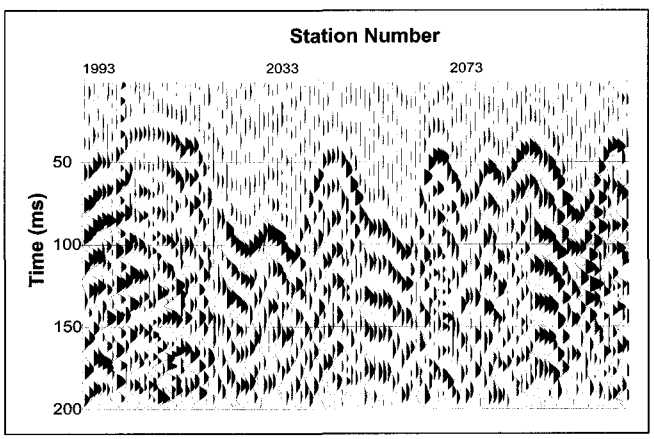

Fig. 11. The RCS generated from the two shot records in Figures 9 and 10 with an 80-m XY value. This RCS has better than average signal-to-noise ratios.

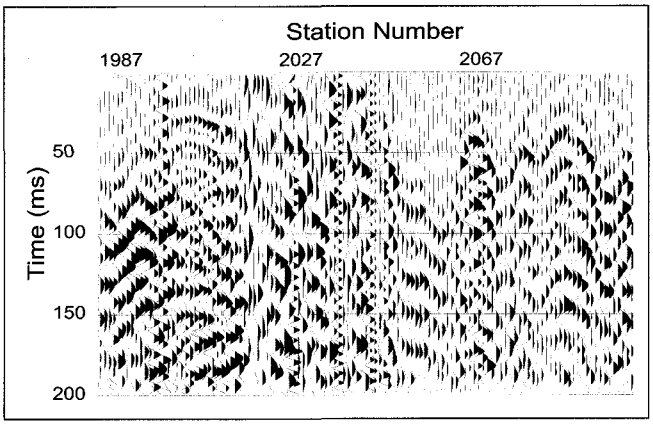

Fig. 12. A more typical RCS. The noisy traces are mainly caused by vehicular traffic along the survey line.

COMPARISON OF REFRACTION STATICS

Figure 14 shows the statics corrections computed with the method of Taner et al. (1998), the GRM, and the RCS. In general, there is excellent agreement. Figure 15 shows the differences between the GRM and the Taner et al. (1998) sets of corrections. There is a long-wavelength difference of about 2 ms at station 1880, which systematically increases to about 4 ms at station 2100, and which is probably the result of using a single constant seismic velocity for the weathering. However, between stations 2020 and 2030, the difference is about 9 ms.

Figure 16 shows the differences between the final statics model, and the two refraction models. While the differences are generally less than about 5 ms, those derived from the GRM model tend to be less than those derived from the Taner et al. (1998) model. Furthermore, the GRM has significantly smaller residuals between stations 2020 and 2030. The RCS residuals are similar to those of the GRM.

There is a negative correlation between the statics and the residual values. This suggests that the average seismic velocity used for the weathered layer may be inaccurate. Figure 17 shows the residual values for the GRM derived statics using two seismic velocities of 700 m/s ($K = 0.884$) and 1700 m/s ($K = 0.735$) in the weathered layer. Those residuals derived with the lower seismic velocity show less correlation with the statics corrections.

DISCUSSION

In this study, the depths of the weathered layer range from 20 m to 148 m, frequently over distances as short as 500 m, or 12 receiver arrays. As a result, the statics corrections range from less than 10 ms to more than 70 ms. This study is another demonstration of the importance in obtaining accurate initial refraction models of the weathering in hard rock terrains where residual statics routines may fail.

Despite the large and rapid variations in the depth of weathering, the simple refraction model of the weathering used in the GRM and the RCS approaches is able to generate refraction statics models which are comparable in accuracy to results generated with a more complex model of the weathering, and a more computationally intensive approach to deriving that model using a least-mean-squares inversion with the conjugate gradient algorithm. The differences between each refraction model systematically vary from an average of 2 ms to 4 ms over a distance of 8.8 km.

The differences between the different refraction models and the final statics model which includes the automatic residual values are generally less than 5 ms. Often the GRM and the RCS models result in smaller residual statics values. Lowering the seismic velocity in the weathered layer reduces the magnitude of the residual statics. These results suggest that short-wavelength statics may often be caused by inaccurate determinations of the average seismic velocity in the weathered layer.

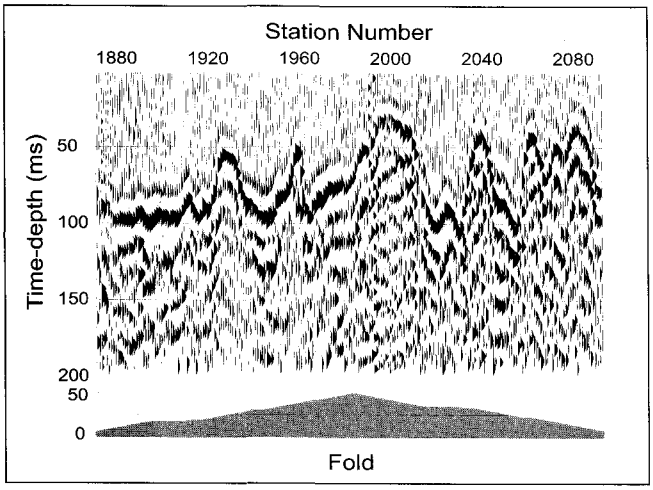

Fig. 13. The final RCS obtained by stacking approximately 50 individual overlapping RCSs. Apart from a few stations near station 2000 where there is no data, stacking has produced an RCS that has good signal-to-noise ratios, even at the ends of the line where the fold is low.

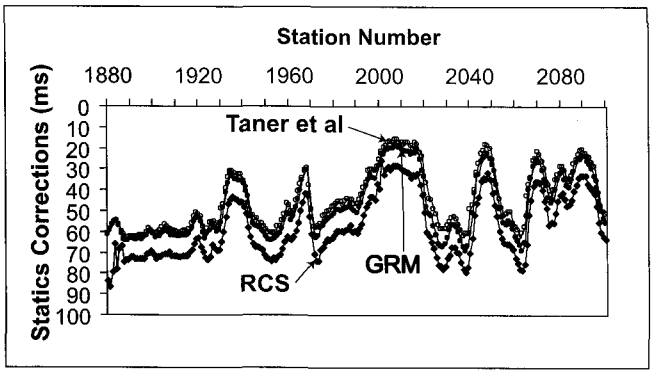

Fig. 14. Refraction statics models computed with the method of Taner et al. (1998) (open circles), the GRM (closed circles), and the RCS (closed diamonds). In general, the agreement is very close.

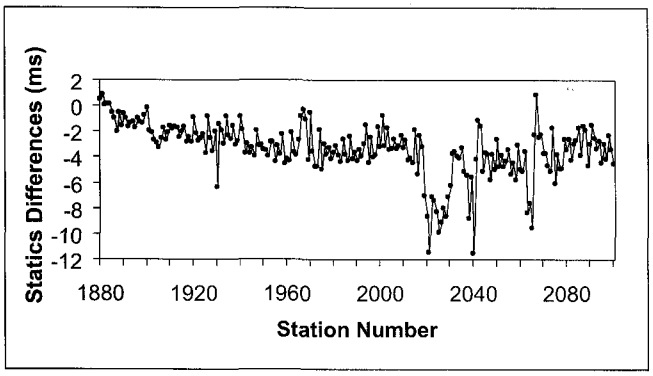

Fig. 15. Differences in statics corrections computed with the GRM and the method of Taner et al. (1998). The differences are approximately 2 ms for the low station numbers and increase to about 4 ms for the high station numbers. However, between stations 2020 and 2030, the differences average about 9 ms.

An essential component in achieving the accurate refraction model with the GRM is the use of the time-depth algorithm, which provides an exact analysis of the traveltime data into averaged delay times between pairs of source points. However, unlike many other refraction algorithms, it requires explicit identification of forward and reverse traveltimes, within the algorithm, and therefore processing of the refraction data in pairs of reversed shot records. The use of forward and reverse shot records is also an integral part of the generation of the RCS.

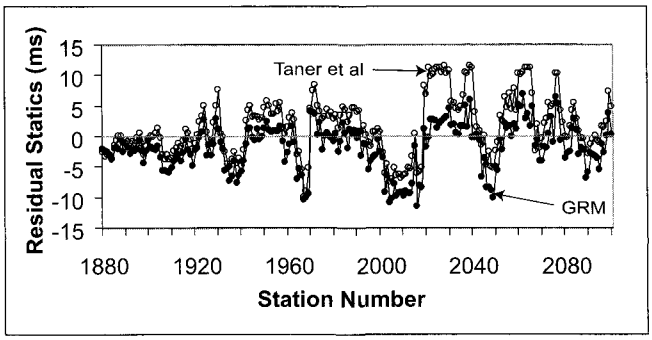

Fig. 16. Differences between the final statics corrections, which include the residual values, and the refraction models computed with the GRM (closed circles) and the method of Taner et al. (1998) (open circles). The differences are generally less than 5 ms. However, between stations 2000 and 2030, the differences are up to 10 ms.

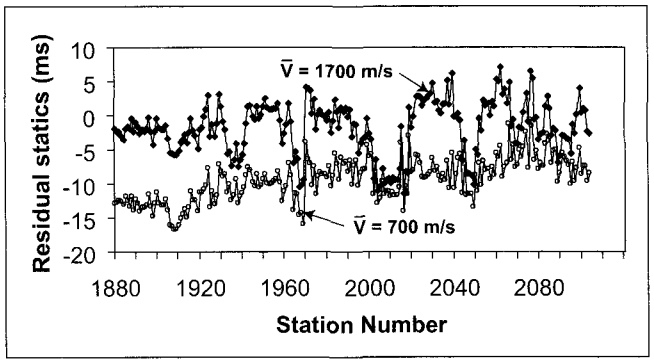

Fig. 17. Residual statics computed with the GRM statics using average weathering velocities of 1700 m/s and 700 m/s. The residuals obtained with the lower average weathering velocity are smaller and show less correlation with the original refraction statics model.

The variable refraction migration operation of the GRM, which is achieved by varying the *XY* distance, also provides a convenient approach to accommodating the finite length of the receiver array, provided of course that end-to-end receiver arrays are employed. With no accommodation of the receiver array, a large segment of the refractor is effectively averaged, and for the set of data used in this study, there can often be large variations in depths of weathering over that interval. A refraction migration distance of one receiver array length generates averaged delay times at the ends of the arrays, and demonstrates that differential statics across individual receiver arrays of more than 5 ms are not uncommon. These results indicate the importance of determining a single statics value that is appropriate to a limited segment of the refractor beneath the centre of each array. Such a value is readily obtained with a refraction migration distance of two receiver intervals.

Errors in determining reciprocal times, the traveltimes from the forward source point to the reverse source point, are the main source of errors in computing the averaged delay times with the time-depth algorithm. These errors result is a simple constant vertical time shift to all of the values computed with a given pair of shot records. The correction is readily obtained by simple subtraction of the values computed with adjacent pairs of shot records. The values, which have been corrected for reciprocal time errors, are then averaged at each station for the complete ensemble of shot pairs.

The significance of this study is that the resolution of the RCS model of the weathering is equivalent to that achieved with the GRM and other detailed refraction methods. The RCS is well suited to achieve further improvements in resolution through

stacking to improve signal-to-noise ratios prior to the measurement of any traveltimes, and with seismic imaging techniques (Taner et al., 1992; Taner et al., 1998; Cox, 1999 p.218–219). In addition, the RCS may facilitate the generation of alternate refraction models of the weathering, such as with shear waves, for which the signals usually occur as relatively low amplitude second arrivals.

CONCLUSIONS

We demonstrate that the simple refraction model of the weathering used with the GRM and the RCS is able to generate refraction statics models that are comparable to results generated with a more complex model of the weathering, and with a more computationally intensive approach to deriving that model using least-mean-squares inversion with the conjugate gradient algorithm. The extension of the GRM to the RCS may facilitate the development of more detailed images of the weathered layer.

ACKNOWLEDGEMENTS

Special thanks to ANSIR and the former director of ANSIR, Barry Drummond, and to Ted Tyne, Director of the NSW Geological Survey for support with data and for facilitating research. Leonie Jones publishes with the permission of the CEO of Geoscience Australia.

Jacques Jenny of W_Geosoft generously provided a copy of Visual_SUNT.

REFERENCES

Barry, K.M., 1967, Delay time and its application to refraction profile interpretation: in Musgrave, A.W., (ed.), *Seismic refraction prospecting*: Society of Exploration Geophysicists, pp.348–361.

Cox, M.J.G., 1999, *Statics corrections for seismic reflection surveys*: Society of Exploration Geophysicists.

Gardner, L.W., 1939, An areal plan of mapping subsurface structure by refraction shooting: *Geophysics*, **4**, 247–259.

Gardner, L.W., 1967, Refraction seismograph profile interpretation: in Musgrave, A.W., (ed.), *Seismic refraction prospecting*: Society of Exploration Geophysicists, pp.85–118.

Glen, R.A., Korsch, R.J., Jones, L.E.A., and Johnston, D.W., 2000, Seismic evidence for a major arc-back arc collision in the Lachlan Orogen: *15th Australian Geological Convention, Geological Society of Australia*, **59**, 177.

Jones, L.E.A., and Drummond, B.J., 2001, Effect of smoothing radius on refraction statics corrections in hard rock terrains: *15th Geophysical Conference and Exhibition, Australian Society of Exploration Geophysicists.*

Kvasnicka, M., and Cerveny, V., 1996, Analytical expressions for Fresnel volumes and Interface Fresnel zones of seismic body waves. Part 2: Transmitted and converted waves. Head waves: *Studia Geophysica et Geodaetica*, **40**, 381–397.

Palmer, D., 1980, *The generalized reciprocal method of seismic refraction interpretation*: Society of Exploration Geophysicists.

Palmer, D., 1986, *Refraction seismics: the lateral resolution of structure and seismic velocity*: Geophysical Press.

Palmer, D., 1992, Is forward modeling as efficacious as minimum variance for refraction inversion?: *Exploration Geophysics*, **23**, 261–266.

Palmer, D., Goleby, B., Drummond, B., 2000, The effects of spatial sampling on refraction statics: *Exploration Geophysics*, **31**, 270–274.

Palmer, D., 2001b, Resolving refractor ambiguities with amplitudes: *Geophysics*, **66**, 1590–1593.

Palmer, D., 2001a, Imaging refractors with the convolution section: *Geophysics*, **66**, 1582–1589.

Palmer, D., 2001c, A new direction for shallow refraction seismology: integrating amplitudes and traveltimes with the refraction convolution section: *Geophysical Prospecting*, **49**, 657–673.

Taner, M.T., Matsuoka, T., Baysal, E., Lu, L., and Yilmaz, O., 1992, Imaging with refractive waves: *62nd Annual International Meeting & Exposition, Society of Exploration Geophysicists.*

Taner, M.T., Wagner, D.E., Baysal, E., Lee, L., 1998, A unified method for 2-D and 3-D refraction statics: *Geophysics*, **63**, 260–274.

GRM 法と RCS 法を用いた屈折静補正の簡易手法

D. パーマー[1]・L. ジョーンズ[2]

要　旨： 地表の風化層が厚くかつ水平方向に急激に変化する硬岩地域で記録された地震探査データに対して、屈折法による静補正値の算出を行った。そのような地域のデータの場合、受振器間隔の 12 倍ほどの短距離では、静補正値は 10 ms 未満から 70 ms 以上まで変化することがしばしばである。この研究では、自動残余静補正が必ずしも有効に働かない硬岩地帯の風化層では、屈折面の初期モデルの正確さが重要であることを示す。

一般化相反屈折法(GRM)および屈折重畳セクション法(Refraction Convolution Section: RCS)を用い単純な風化層モデルに対して計算された静補正値と、CG 法を利用した最小二乗インバージョンを用いて複雑な風化モデルについて計算された静補正値は、ほぼ同等の正確さを有する。両者による静補正値の違いは、8.8 km 以上の距離にわたって系統的に平均 2- 4 ms 程度であった。これら 2 つの屈折モデルと自動残余静補正を含めた最終の静補正値モデルの間の差は、一般に 5 ms 未満であった。

GRM モデルによる残余静補正はしばしば CG 法モデルによる補正より小さくなる。RCS による静補正はおよそ 10 ms 遅れるが、それらの相対的な精度は GRM 静補正のそれと同等である。残余静補正値は、屈折法による静補正値と一般によい相関を示し、風化層の平均地震波速度を遅く仮定することにより、その補正値を減らすことができる。この結果、静補正値の短波長変化の原因が、走時から平均遅れ時間を決定する逆解析アルゴリズム中の欠点によるものではなく、風化層の平均地震波速度の不正確な推定によるものであることがわかる。

GRM과 RCS 방법을 이용한 굴절파 정적 시간차를 구하는 간단한 방법

Palmer, D[1]・Jones, L[2]

요　약： 풍화대의 심도가 급변하는 경암지형에서 얻은 자료로부터 굴절파의 정적 시간차(refraction statics)들이 계산되었다. 정보정값은 수신기 간격들의 12 배 정도되는 거리에 대해 보통 10 ms 이하에서 70 ms 이상의 값을 가진다. 이 논문에서는 자동 잔여 시간차가 항상 유용하지만은 않은 경암 지형에서 풍화대의 정확한 초기 굴절법 모델을 얻는 것이 얼마나 중요한 가에 대한 한 예를 보여주고 있다.

GRM 과 RCS (Refraction Convolution Section)법을 이용해 구한 간단한 풍화대 모델의 시간차 값들과 CG 법(Taner et al., 1998)을 이용한 최소 평균 제곱 역산에 의해 좀 더 복잡한 풍화대 모델에 대해 구해진 값들을 정확도 면에서 비교될 만하다. GRM 모델과 Taner 모델은 8.8 km 거리에 대해 체계적으로 평균 2 내지 4 ms 의 차이가 났다. 이들 두 모델들과 자동 잔여값을 포함한 최종 시간차 사이의 차이는 일반적으로 5 ms 이내이다.

GRM 모델에서의 잔여값들은 때때로 Taner et al.(1998)의 모델의 잔여값들보다 작다. RCS 법에서의 시간차들은 대략 10 ms 뒤에 발췌되지만 상대적인 정확도는 GRM 시간차들에 견줄만하다.

잔여 시간차값들은 굴절파 시간차값들과 일반적으로 상관관계를 보이며, 풍화대에서 더 낮은 탄성파 평균 속도를 이용함으로써 그 크기를 줄일 수 있다. 이들 결과들을 통해 풍화대에 적용된 부정확한 탄성파 평균 속도들은, 주시로부터의 평균지연시간을 결정하는 역산 알고리듬의 어떤 문제점들보다도, 짧은 파장의 시간차의 원인이 될 수 있음을 알 수 있다.

1 School of Biological, Earth and Environmental Sciences, the University of New South Wales
Sydney, NSW 2052, Australia
2 Geoscience Australia

1 ニューサウスウエルズ大学　生物学・地球・環境学部
2 ジオサイエンス・オーストラリア